Spin diffusion on a lattice: Classical simulations and spin coherent states

Daniel K. Sodickson and John S. Waugh
Division of Health Sciences and Technology and Department of Chemistry, Massachusetts Institute of Technology, Cambridge, Massachusetts 02139

(Received 22 December 1994; revised manuscript received 15 May 1995)

The results of computational studies of classical spin diffusion on a lattice are presented, and the validity of these results in the quantum regime is explored using a general theoretical framework. First, classical simulations of spin diffusion are used to identify conservation principles required for adherence to a traditional diffusion equation. The breakdown of diffusive behavior for magnetization in zero applied field is tied to nonconservation of spin angular momentum by the dipole-dipole interaction. The effects of dilution upon the spin diffusion constant are also studied for lattices of various dimensionalities. At low concentrations and low dimensionality, the results are suggestive of percolation. Next, with considerations of spin diffusion serving as a model, classical spin dynamics on a lattice are linked to quantum dynamics using the interpolating properties of spin coherent states. For systems with initial disturbances characterized by slow spatial variation, and in the limit of high temperature and large particle number, a full quantum treatment of the spin diffusion problem is shown to reduce to the classical paradigm used in numerical simulations. The equivalence of quantum and classical behaviors under these conditions is shown to result from the cancellation of quantum interference terms in the coherent-state representations of expectation values.

I. INTRODUCTION

Several approximate analytic theories for spatial spin diffusion exist and are in rough agreement with experiment, but many of the details of the spin diffusion process remain to be explored. As a consequence, a classical simulation was recently developed to investigate the dynamics of spin diffusion in lattices.[1,2] Using a model of classical gyromagnets precessing in each others' dipole fields, Tang and Waugh derived numerical values for the spin diffusion constant in model lattices, and characterized several of the main conceptual and computational issues for classical spin diffusion. Their results were generally in good agreement both with theory[3–8] and with experiment.[9] Given the success of these initial calculations, we have undertaken to study aspects of spin diffusion which are not readily accessible to current analytic theories but which shed light upon the microscopic foundations of the phenomenon. The classical simulations are here extended to new situations of interest in solid-state NMR and condensed-matter physics, namely, the cases of spin lattices in zero or small external magnetic field (Sec. II), and of lattices randomly diluted with vacancies or nonmagnetic impurities (Sec. III).

Section IV is devoted to reconciling quantum theories with classical simulations using the quasiclassical properties of spin coherent states. Use of these states in formulating the quantum spin diffusion problem affords a direct comparison with classical dynamical models, giving credence to the results of classical simulations in situations where their validity is otherwise difficult to verify. A study of the conditions under which classical results are recovered from the quantum formalism also serves to indicate at what points quantum behaviors would be expected to diverge from their classical counterparts.

II. THE EFFECTS OF APPLIED MAGNETIC FIELD UPON SPIN DIFFUSION

Tang and Waugh showed that in the presence of a strong applied magnetic field, both longitudinal magnetization and dipolar interspin energy display demonstrably diffusive dynamics.[1,2] That this is so is most easily ascertained by observing the behavior of these quantities as a function of spatial frequency. Given a diffusion equation for spin magnetization,

$$\frac{\partial M(\boldsymbol{r},t)}{\partial t} = \sum_{\mu} D_{\mu\mu} \frac{\partial^2 M(\boldsymbol{r},t)}{\partial x_{\mu}^2} \tag{2.1}$$

and its spatial Fourier transform

$$\begin{aligned} \frac{\partial A_M(\boldsymbol{k},t)}{\partial t} &= -\sum_{\mu} k_{\mu}^2 D_{\mu\mu} A_M(\boldsymbol{k},t) \\ &= -k^2 D_{\hat{k}} A_M(\boldsymbol{k},t), \end{aligned} \tag{2.2}$$

an initial disturbance amplitude $A_M(\boldsymbol{k},t)$ at any given spatial frequency k is expected to decay exponentially with a rate proportional to k^2. Here the diffusion equation has been written in the principal axis system of the diffusion tensor $\overleftrightarrow{D}$, with Cartesian axes labeled $x_\mu (\mu = 1,2,3)$. The diffusion constant $D_{\hat{k}} \equiv \sum_\mu (k_\mu^2/k^2) D_{\mu\mu}$ depends only upon the direction $\hat{k}$ along which the amplitude $A_M(\boldsymbol{k},t)$ is measured. A similar expression may be written for the amplitude A_E of interspin energy. Tang and Waugh demonstrated that the decays of both A_M and A_E scale appropriately as k^2 in high field. Both quantities therefore obey a diffusion equation, and in each case a single diffusion constant D_M or D_E can be defined for all wavelengths $\lambda = 2\pi/k$ of the initial disturbance.

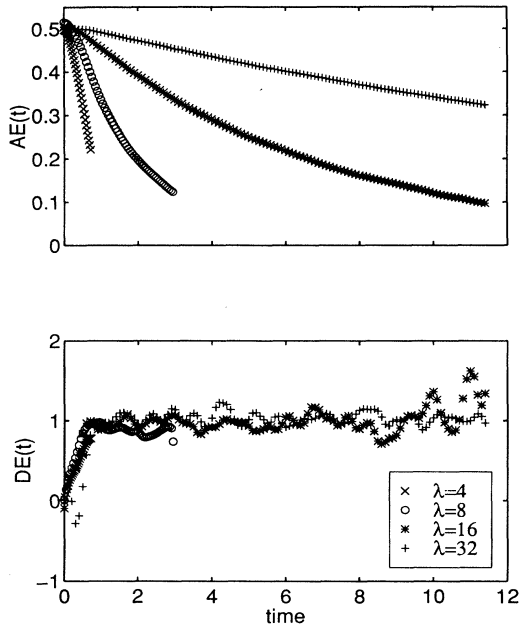

FIG. 1. Wavelength dependence of disturbance amplitude $A_E(t)$ and diffusion constant $D_E(t)$ for interspin energy in zero applied field. Diffusion is measured along the [100] axis of a simple cubic lattice ($16 \times 16 \times 16$ spins for $\lambda = 4, 8, 16$, and $32 \times 16 \times 16$ for $\lambda = 32$). Plotted curves are averages of 64 runs.

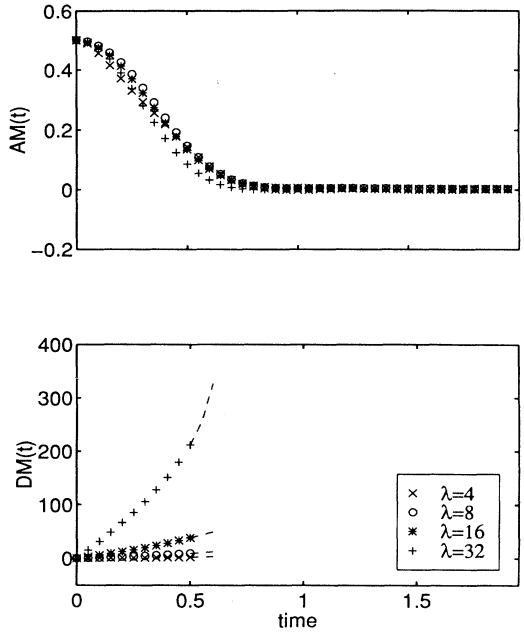

FIG. 2. Wavelength dependence of disturbance amplitude $A_M(t)$ and diffusion constant $D_M(t)$ for magnetization in zero applied field. Other simulation parameters as in Fig. 1.

Similar results are obtained here for the diffusion of interspin energy in zero applied magnetic field. Figure 1 shows the scaling of $A_E(t)$ and $D_E(t)$ [the instantaneous diffusion coefficient calculated using Eq. (2.2)] over four octaves from $\lambda = 4$ to $\lambda = 32$. The computational strategy for these simulations was outlined in Ref. 1 and will be reviewed briefly in Sec. IV. More detailed methodological discussions may be found in Refs. 2 and 10. Only the principal results will be presented here.

After an initial induction time,[2,10] the diffusion coefficient remains essentially constant for all the wavelengths tested. Its numerical value[11] is significantly larger than for a similar lattice in high field (Table I), since the external field acts as an impediment to dipole-driven magnetization exchange.

By contrast, the tranport of spin magnetization is *not* diffusive in zero field, as is demonstrated by Fig. 2. For wavelengths from $\lambda = 4$ to $\lambda = 32$, the spin polarization amplitude $A_M(t)$ decays at a uniform rate, and no single consistent diffusion constant can be defined.

TABLE I. Diffusion constants for interspin energy in zero field and in high field, measured in reduced units (see Ref. 11). The high field values (from Ref. 2) are for diffusion parallel ($D_{E\parallel}$) and perpendicular ($D_{E\perp}$) to an applied field along the [100] lattice direction. The average diffusion constant $\bar{D}_E = \frac{2}{3}D_{E\perp} + \frac{1}{3}D_{E\parallel}$ is also included.

Zero field (this work)	High field (Ref. 2)		
D_E	$D_{E\parallel}$	$D_{E\perp}$	$\bar{D}_E$
0.99	0.63	0.19	0.34

This discrepancy between high-field and zero-field behaviors may be understood by considering the influence of an applied magnetic field upon the efficacy of the dipole coupling. The Hamiltonian for a dipole-coupled spin system in the presence of an external magnetic field $\boldsymbol{B}_0$ may be written as follows:

$$\mathcal{H} = -\sum_j \boldsymbol{m}_j \cdot \boldsymbol{B}_0 - \frac{1}{2}\sum_j \sum_{k\neq j} \frac{1}{{r_{jk}}^3} \times [3(\boldsymbol{m}_j \cdot \hat{\boldsymbol{r}}_{jk})(\boldsymbol{m}_k \cdot \hat{\boldsymbol{r}}_{jk}) - \boldsymbol{m}_j \cdot \boldsymbol{m}_k]. \quad (2.3)$$

In high field (large $\boldsymbol{B}_0$), this Hamiltonian may be truncated to the following form (in the rotating frame of $\boldsymbol{B}_0$):[12]

$$\mathcal{H} = -\frac{1}{2}\sum_j \boldsymbol{m}_j \cdot \boldsymbol{B}_j^{\text{trunc}}$$

$$\boldsymbol{B}_j^{\text{trunc}} = \sum_{k\neq j} \frac{3\cos^2\theta_{jk} - 1}{2{r_{jk}}^3}(m_{k_x}\hat{\boldsymbol{x}} + m_{k_y}\hat{\boldsymbol{y}} - 2m_{k_z}\hat{\boldsymbol{z}}). \quad (2.4)$$

Here, r_{jk} and θ_{jk} represent the magnitude and orientation of the vector $\boldsymbol{r}_{jk}$ connecting spins $\boldsymbol{m}_j$ and $\boldsymbol{m}_k$. The presence of a strong applied field serves to identify the z component of magnetization with a large energy—the Zeeman energy—and the high-field truncation is designed such that only motions conserving this energy are allowed. In high field, then, the z component of spin angular momentum (which corresponds in a lattice of like

spins to the longitudinal spin magnetization) is effectively conserved.

In the absence of an applied magnetic field, the dipole Hamiltonian takes its full untruncated form

$$\mathcal{H} = -\frac{1}{2}\sum_j \boldsymbol{m}_j \cdot \boldsymbol{B}_j^{\text{untrunc}},$$
$$\boldsymbol{B}_j^{\text{untrunc}} = \sum_{k\neq j} \frac{1}{{r_{jk}}^3}[3(\boldsymbol{m}_k \cdot \hat{\boldsymbol{r}}_{jk})\hat{\boldsymbol{r}}_{jk} - \boldsymbol{m}_k]. \quad (2.5)$$

One might argue that the zero-field dipole coupling is a purely internal interaction, which can exert no net torque on the system as a whole. According to this argument, the total angular momentum, and the magnitude of each of its components, should be conserved. Nevertheless, the form of $\mathcal{H}$ in zero field is somewhat suspicious: it contains all the elements of the traditional dipolar alphabet, including terms representing uncompensated single or double spin "flips" which do not preserve any single component of angular momentum. Considering for the moment a simplified two-spin system, $\boldsymbol{m}_1$ and $\boldsymbol{m}_2$, and writing the usual Bloch equations with untruncated dipole fields from Eq. (2.5), we find that

$$\begin{aligned}\frac{d\boldsymbol{J}_{\text{spin}}}{dt} &= \frac{d}{dt}(\boldsymbol{m}_1 + \boldsymbol{m}_2) = \gamma(\boldsymbol{m}_1 \times \boldsymbol{B}_1 + \boldsymbol{m}_2 \times \boldsymbol{B}_2) \\ &= \frac{\gamma}{r_{12}^3}[\boldsymbol{m}_1 \times (3\hat{\boldsymbol{r}}_{12}(\boldsymbol{m}_2 \cdot \hat{\boldsymbol{r}}_{12}) - \boldsymbol{m}_2) \\ &\qquad + \boldsymbol{m}_2 \times (3\hat{\boldsymbol{r}}_{12}(\boldsymbol{m}_1 \cdot \hat{\boldsymbol{r}}_{12}) - \boldsymbol{m}_1)] \\ &= \frac{3\gamma}{r_{12}^3}[(\boldsymbol{m}_1 \times \hat{\boldsymbol{r}}_{12})(\boldsymbol{m}_2 \cdot \hat{\boldsymbol{r}}_{12}) \\ &\qquad + (\boldsymbol{m}_2 \times \hat{\boldsymbol{r}}_{12})(\boldsymbol{m}_1 \cdot \hat{\boldsymbol{r}}_{12})] \\ &\neq 0\,. \end{aligned} \quad (2.6)$$

For a general orientation of the two dipoles $\boldsymbol{m}_1$ and $\boldsymbol{m}_2$, $\boldsymbol{J}_{\text{spin}}$ is not conserved. Under the action of the zero-field dipole-dipole Hamiltonian, angular momentum conservation cannot be maintained within the bounds of spin space alone.

To recover the lost momentum, we must turn to coordinate space. By a quick commutator calculation, or else by an appeal to Ehrenfest's theorem, we can derive a quantum result equivalent to that of Eq. (2.6). Then, using the commutation relations of the relative position and momentum vectors $\boldsymbol{r}_{12}$ and $\boldsymbol{p}_{12}$, we find that

$$\frac{d\boldsymbol{L}_{\text{coor}}}{dt} = \frac{i}{\hbar}[\mathcal{H}, \boldsymbol{r}_{12} \times \boldsymbol{p}_{12}] = -\frac{d\boldsymbol{J}_{\text{spin}}}{dt}, \quad (2.7)$$
$$\frac{d\boldsymbol{J}_{\text{tot}}}{dt} = \frac{d}{dt}(\boldsymbol{J}_{\text{spin}} + \boldsymbol{L}_{\text{coor}}) = 0. \quad (2.8)$$

If the two spins were not held fixed in space, the net torque generated by the dipolar interaction between them would serve to rotate their interspin vector $\boldsymbol{r}_{12}$ so as to compensate for the change in spin angular momentum. These arguments can be generalized without complication to our many-spin lattice, for which we conclude that spin angular momentum is *not* conserved in zero field, but rather exchanges continually with the collective orbital angular momentum of the lattice (or is absorbed through external torques if the lattice is held fixed). Spin space and coordinate space are both represented in the dipole-dipole Hamiltonian, and though these two spaces are customarily considered separately, we cannot account fully for the dynamics of our spins without appealing to both.

The fact that the zero-field dipole coupling does not conserve magnetization (or spin angular momentum) has been appreciated for some time, and has been found to have a significant influence on the critical dynamics of dipolar ferromagnets.[13–15] Not surprisingly, this elementary property also has important implications for spin diffusion in zero field. Diffusion, at least in the strict sense embodied by the diffusion equation, is founded upon conservation principles. Diffusive transport is always driven by a gradient in some globally conserved quantity. The canonical example is the diffusion of gas along a concentration gradient. There, the diffusion equation may be derived directly from the continuity equation for mass flow through a given region of space. If the constraints of mass conservation (or conservation of total particle number) are lifted, the gas transport is no longer strictly diffusive. Similar arguments can be adduced for spin diffusion. In high field, Zeeman energy and interspin energy are independently conserved. Both therefore diffuse according to a classical diffusion equation. In zero field, however, while interspin energy is still conserved, there is no conserved Zeeman energy, and hence no conserved component of spin angular momentum. Not only can net magnetization in a given direction flow from regions in which it is abundant to other regions in which it is scarce, but it can also disappear into the "sink" of lattice rotation, or can equilibrate among the other magnetization directions.

Simulations in fields of moderate strength, intermediate between the high-field and zero-field extremes, confirm the importance of angular momentum conservation in the bulk dynamics of the spin lattice. In this case, neither Zeeman energy nor dipole-dipole energy is independently conserved; only their sum, the total magnetic energy, remains constant over time. The transport behavior of each of these three energies—Zeeman, dipole, and total—is summarized in Fig. 3. For all of these intermediate-field simulations, the untruncated dipole coupling was supplemented by an external field (oriented parallel to the diffusion axis in the z direction) at five times the magnitude of the nearest-neighbor dipole coupling. The total local dipole field felt by any spin is generally a few times larger than the nearest-neighbor field, and the applied field was chosen to lie in this range. At short times (shorter than the induction time of roughly one reduced unit), the amplitudes of both Zeeman and dipole energy decay at a rate nearly independent of wavelength, reminiscent of the decay of Zeeman amplitude in Fig. 2. At longer times, the curves for different wavelengths do disperse, but not enough to define a single diffusion constant. The amplitude of total magnetic energy, on the other hand, adheres closely to a diffusive profile.

Results at other intermediate field values show that diffusion behavior continues to track conservation. At very low fields, it is magnetization which "misbehaves,"

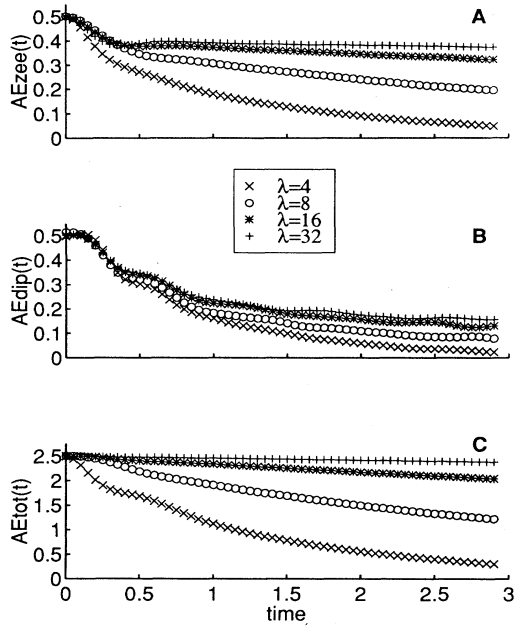

FIG. 3. Wavelength dependence of disturbance amplitudes $A_{E_{\rm zee}}(t)$, $A_{E_{\rm dip}}(t)$, and $A_{E_{\rm tot}}(t)$ for Zeeman energy (a), dipole energy (b), and total magnetic energy (c) in intermediate applied field. Other simulation parameters as in Fig. 1.

while dipole energy, which constitutes the bulk of the total energy, is nearly conserved and diffuses accordingly. As the applied field grows, the Zeeman energy becomes the principal component of the total, and the dipole energy begins to depart from strictly diffusive behavior. At very high fields, truncation of the dipole interaction takes effect, and the Zeeman and dipole energies each behave diffusively.

III. CONCENTRATION DEPENDENCE OF SPIN DIFFUSION AND THE EFFECTS OF LATTICE GEOMETRY

The simulations described above demonstrate that changes in the functional form of the interaction between neighboring spins (effected by changes in the strength of the applied magnetic field) can have profound effects upon the bulk transport behavior of the lattice. In a second set of simulations, the *distribution* of neighboring spins was varied by varying the population of the model lattice—introducing vacancies at a random subset of lattice sites. These simulations mimic the physical conditions in spin lattices diluted by actual vacancies or by nonmagnetic impurities.

It is not difficult to modify the basic spin diffusion simulation to study the effects of random lattice dilution. One first chooses a target lattice concentration $c_{\rm target}$ between 0 and 1, then one samples a random number generator for each lattice site. If the generator returns a value less than $c_{\rm target}$, the site is populated with a spin. Otherwise, it is left empty. The quantity $c_{\rm target}$ therefore serves as a site occupation probability, and the actual fractional concentration $c = N_{\rm spins}/N_{\rm sites}$ approaches $c_{\rm target}$ as the number of spins becomes large. Nolden and Silbey in 1993 performed dilution studies of this sort in three-dimensional lattices and studied the effects of various lattice parameters upon the computed diffusion constants.[16] In a forthcoming paper,[17] they will present their data from lattices larger than the ones used here.

The concentration dependence of the diffusion constant for spin magnetization in a simple cubic lattice at high applied field is plotted as open circles in Fig. 4. (Here, the actual fractional concentration c is used as the independent variable, rather than the theoretical target concentration.) The diffusion constant is seen to fall monotonically as the lattice is diluted. This behavior is not surprising, since the magnitude of the average local field experienced by any of the spins falls off similarly as spins are removed from the lattice.

The moment theory of Redfield and Yu[5] serves nicely in a first attempt to understand the shape of the $D(c)$ curve, since moments can be expressed as lattice sums whose concentration dependence is easy to ascertain. Redfield and Yu derive the following form for the diffusion constant D_Z of spin magnetization (or Zeeman energy) in high field:

$$D_Z = \left(\frac{M_2}{k^2}\right)\left(\frac{\pi M_2}{2M_4}\right)^{\frac{1}{2}}. \tag{3.1}$$

As usual, k is the wave number of the initial magne-

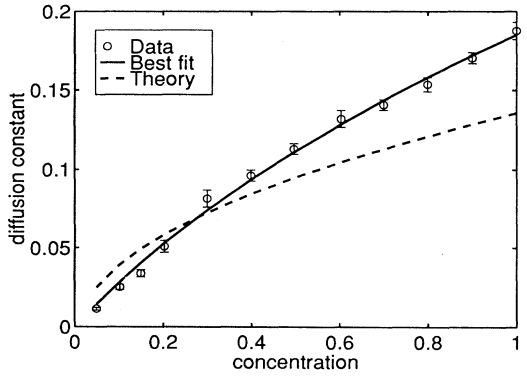

FIG. 4. Concentration dependence of the spin diffusion constant (high-field diffusion of magnetization) in a three-dimensional simple-cubic lattice. Open circles: simulated data. Solid line: best fit of $D(c)$ to Eq. (3.5). Dashed line: exact results of the Redfield and Yu moment theory [Eqs. (3.6)]. The size of the lattice is $N_{\rm sites} = 16 \times 16 \times 16$, and the orientation of the applied field is [111]. Diffusion was measured along the [100] axis for an initial spin polarization with $\lambda = 16$. At each concentration, diffusion constants for 8 different runs were obtained as averages of the instantaneous values $D(t)$ over suitable time intervals, and these 8 average values were averaged to yield the value shown in the plot. The error bars indicate standard error of the mean of the 8 samples.

tization disturbance. M_2 and M_4 are the second and fourth moments of an appropriately defined absorption line shape (cf. Ref. 5), and are related (though not identical) to the classic Van Vleck moments.[18] Some algebraic manipulation yields the expression

$$D_Z = \left(\frac{-\frac{\pi}{2} \left(\sum_j' x_{ij}^2 \mathcal{A}_{ij} \right)^3}{\sum_j' \sum_k' x_{ij}^2 \mathcal{B}_{ijk} + \sum_j' x_{ij}^2 \mathcal{C}_{ij}} \right)^{\frac{1}{2}} \qquad ijk \neq, \quad (3.2)$$

where the primed sums run over the occupied lattice sites. $x_{ij}^2 = (x_i - x_j)^2$ are the squared separations of spins i and j in the direction of the initial wave vector, and

$$\mathcal{A}_{ij} = \frac{1}{3} \left(\frac{3\cos^2 \theta_{ij} - 1}{2 r_{ij}^3} \right)^2 \equiv \frac{1}{3} b_{ij}^2, \quad (3.3a)$$

$$\mathcal{B}_{ijk} = \frac{2}{9} \{ 8 b_{ij}^2 \left(b_{ik} - b_{jk} \right)^2 + 4 b_{ij} b_{ik} b_{jk} \left(b_{ik} + b_{jk} \right) - 3 b_{ik}^2 b_{jk}^2 \}, \quad (3.3b)$$

$$\mathcal{C}_{ij} = -\frac{32}{15} b_{ij}^4. \quad (3.3c)$$

We may now argue, following Kittel and Abrahams,[19] that for a randomly diluted crystal with site occupation probability c, each spin on average will see other spins at only a fraction c of the lattice sites, and each primed sum in Eq. (3.2) will be smaller than the corresponding sum over all sites by a factor of c. That is,

$$\sum_j' \rightarrow c \sum_j, \quad (3.4a)$$

$$\sum_j' \sum_k' \rightarrow c^2 \sum_j \sum_k. \quad (3.4b)$$

Thus, we may write D_Z in terms of c and the values of the (unprimed) lattice sums at full lattice population. The result is

$$D_Z = \frac{\chi_1 c}{(1 + \chi_2 c)^{\frac{1}{2}}}, \quad (3.5)$$

with

$$\chi_1 = \left(\frac{\frac{\pi}{2} \left(\sum_j x_{ij}^2 \mathcal{A}_{ij} \right)^3}{-\sum_j x_{ij}^2 \mathcal{C}_{ij}} \right)^{\frac{1}{2}}, \quad (3.6a)$$

$$\chi_2 = \frac{\sum_j \sum_k x_{ij}^2 \mathcal{B}_{ijk}}{\sum_j x_{ij}^2 \mathcal{C}_{ij}} \qquad ijk \neq . \quad (3.6b)$$

Figure 4 compares the simulated data with the predictions of the Redfield and Yu theory. A nonlinear least-squares fit of the data to the functional form of Eq. (3.5) yields excellent agreement (solid line in Fig. 4). The best-fit parameters χ_1 and χ_2 do not match the predicted values from Eq. (3.6), however: the moment calculations predict a smaller diffusion constant at full concentration and a smaller initial slope than are observed in the simulations (dashed line in Fig. 4).

What accounts for the residual discrepancy between the simulated and the predicted shapes of the concentration dependence? First of all, the Redfield and Yu moment theory is of course an approximation. There is latitude, for example, in the choice of line shape leading to an expression such as Eq. (3.1). Second, the finite lattice size used in our calculations may be a limitation: the moments of Eq. (3.1) are evaluated in the long-wavelength limit, while a lattice size of $N = 16^3$ and a wavelength of $\lambda = 16$ may fall slightly short of this limit. Also, the summation arguments of Eq. (3.4) become less accurate and the lattice calculations themselves become less precise as the particle number decreases for small c. Whether or not these factors are sufficient to explain the numerical discrepancy, one may also note that the reasoning leading to Eq. (3.5) makes no reference to the *dimensionality* of the lattice. The summation arguments of Eq. (3.4) apply equally well whether the spins are arranged in a line, a plane, or a cube. (Indeed, our moment theory has the character of a "mean field" approach neglecting fluctuations, and therefore no dimension dependence is to be expected.) We know, however, that the dipole interaction falls off as the cube of the interspin distance: although in three dimensions it is a borderline long-range interaction (its volume integral for a constant spin density is logarithmically divergent), it does not remain so in one or two dimensions. As the effective range of the interaction is decreased, percolation theory[20] would suggest that diffusion should no longer scale uniformly with dilution, but should instead show signs of a percolation threshold.

Simulations in one, two, and three dimensions yield the results displayed in Fig. 5. There is a marked difference in the shape of the $D(c)$ curves for the different dimensional-

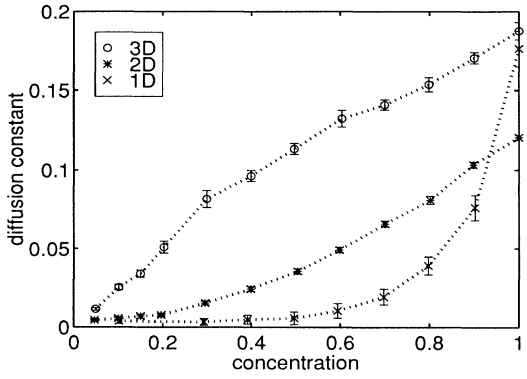

FIG. 5. Concentration dependence of the spin diffusion constant in one, two, and three dimensions. Error bars indicate standard error of the mean; dotted lines are drawn between data points to guide the eye. 3D: 8 runs, $N_{\text{sites}} = 16 \times 16 \times 16$, $\lambda = 16$, field orientation [111], diffusion direction [100]. 2D: 16 runs, $N_{\text{sites}} = 64 \times 64$, $\lambda = 16$, field orientation [111], diffusion direction [100]. 1D: 32 runs, $N_{\text{sites}} = 256$, $\lambda = 16$, field orientation and diffusion direction [100]. The one-dimensional (1D) diffusion constant is greater than its 2D counterpart at $c = 1$ because of the field orientation chosen. A [111] field orientation could not be used in the 1D case, since all 1D couplings vanish for that orientation.

ities. Dimension dependence may be introduced into the spin diffusion problem in a preliminary (and highly approximate) fashion by way of a simple scaling argument. If the lattice population is diluted by a factor c, then the average effective volume occupied by any spin increases by a factor of c^{-1}, and the average nearest-neighbor distance r_0 increases by a factor of $c^{-1/d}$, where d is the dimension of the lattice. If we imagine that this *average* effect on interspin distances constitutes the primary effect of the dilution, then we may model the diluted lattice as a fully populated lattice with the same geometry as the original lattice but with an effective lattice spacing of $c^{-1/d}r_0$. The base coupling strength $b(r_0) \propto r_0^{-3}$ is then scaled by $c^{3/d}$, and all characteristic times, including the decay rate $\tau_k = \left(k^2 D\right)^{-1}$, grow by the inverse factor $c^{-3/d}$. The diffusion constant D, therefore, scales with concentration as $c^{3/d}$.

Figure 6 compares the observed $D(c)$ curves with the predictions of the uniform scaling model on the one hand and the Redfield and Yu moment theory on the other. While the moment arguments, as we have already seen, predict some of the essential features of the three-dimensional curve, scaling arguments are much more successful in one and two dimensions. Even then, however, the fit is not perfect: especially in one dimension, the simulated $D(c)$ falls off significantly faster than c^3, and, of course, in no instance does the scaling model predict anything like a percolation threshold. Even though scaling arguments do account for lattice dimension in a somewhat artificial manner, they take no more account

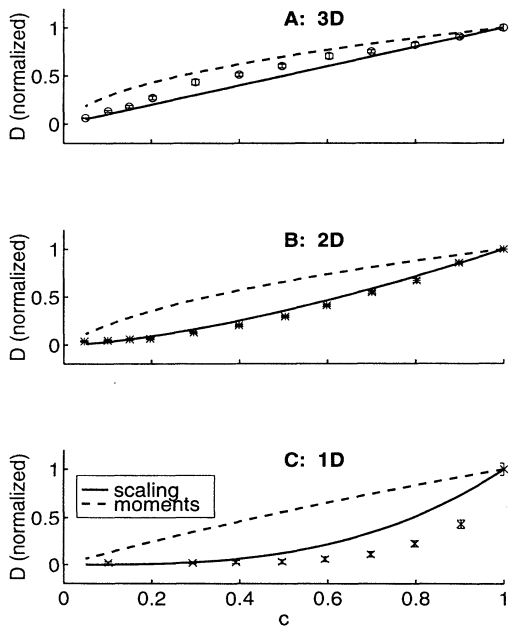

FIG. 6. Comparison of simulated $D(c)$ curves from Fig. 5 (normalized to unity at $c = 1$) with the predictions of moment theory and of uniform scaling arguments described in the text. (a) Three dimensional lattice. (b) Two-dimensional lattice. (c) One-dimensional lattice.

of fluctuations in lattice spacing than does the moment approach. In order to address the detailed dynamics of a randomly diluted lattice, we should consider percolative properties.

For our diffusing spin system, we would expect a percolation threshold to be marked by two kinds of effects. First, for moderate dilutions, a falloff in the observed diffusion constant at long times should accompany the onset of restricted diffusion. Some behavior of this sort is observed in the simulated diffusion constant data, though the presence of an initial induction time and of statistical fluctuations in $D(t)$ complicate these observations. Second, when cluster sizes are small enough (with an average length scale significantly smaller than the wavelength of the magnetization disturbance, for example), spin diffusion will be quenched. In this case, restricted clusters of adjacent spins sit on small portions of the initial disturbance profile, and there is no significant local gradient to drive magnetization transport.

Of course, terms such as "cluster size" apply only in a relative sense to a system such as ours with interactions of extended range. Even in a one-dimensional array of spins, magnetization can cross gaps, incurring only the penalty of a time delay. Furthermore, spin diffusion involves continuous rotations rather than discrete jumps, so that diffusion paths are not easy to define, not to mention to enumerate. Even if such paths could be tallied conveniently, they would have to be weighted by the particular magnetization gradients available to drive diffusion. Thus, a full quantitative theory of the percolation properties of our spin system promises to be exceedingly difficult. If we wish to determine with confidence whether there is such a thing as a percolation threshold for dipolar spin diffusion, we are forced to make simplifications.[21]

Figure 7 compares the curves from Fig. 5 with simulation results for a simplified spin system in which nearest-neighbor Heisenberg exchange couplings were used in place of the dipole-dipole couplings. In the Heisenberg-coupled system, quenching of spin diffusion at low concentrations is plain to see for all dimensionalities. In two and three dimensions, the $D(c)$ curve for nearest-neighbor Heisenberg coupling travels with its dipolar counterpart at high concentrations, then descends more steeply toward a distinct threshold. As expected, the quenching of diffusion occurs at higher concentrations in two than in three dimensions, and the divergence between Heisenberg and dipolar behavior is more muted in the planar lattice. The one-dimensional curves are barely distinguishable, suggesting that nearest-neighbor influences are nearly sufficient to explain the effects of dilution in a line of spins. In short, the simplified Heisenberg model reproduces many of the qualitative features of our full dipolar spin system, while emphasizing the role of, as it were, local demographics in the overall population dynamics of the lattice. The concentration dependence of dipolar spin diffusion may then be understood as a kind of "smoothing over" of the percolative behavior of truly local interactions.

It should be cautioned that the interpretation of a macroscopic diffusion constant in diluted lattices is not entirely straightforward, especially in one dimension. In

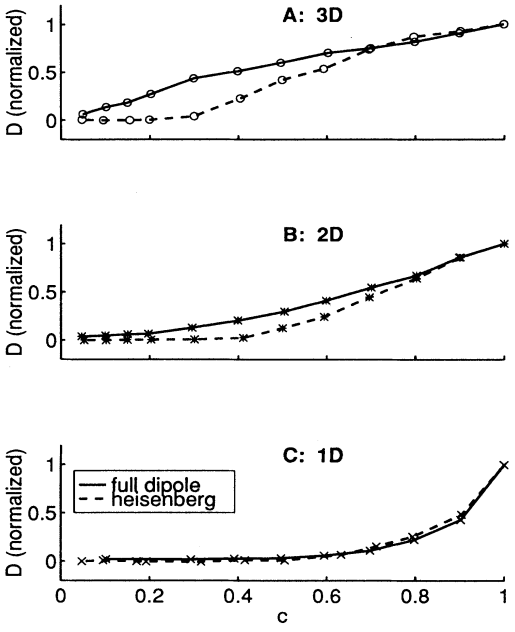

FIG. 7. Comparison of $D(c)$ for dipole couplings (solid lines connecting data points from Fig. 5) and Heisenberg exchange couplings (dashed lines connecting simulated data points). (a) Three-dimensional lattice. (b) Two-dimensional lattice. (c) One-dimensional lattice.

the case of a line of spins subject to nearest-neighbor couplings [as in Fig 7(c)], for example, the theoretical percolation threshold lies at $c = 1$, since the introduction of even a single vacancy necessarily subdivides the system into unconnected clusters. This fact presents both theoretical and practical difficulties. In principle, diffusion in the subdivided system is restricted, and the single bulk diffusion constant should properly by replaced by a distribution of diffusion constants for separate subsystems. Our numerical calculation of the diffusion constant, moreover, involves tracking the amplitude of a single spatial Fourier component across the entire system, but if separate clusters equilibrate to different average values (e.g., if vacancies isolate different segments of the initial cosinusoidal disturbance), then the equilibrium state of the system will contain discontinuities which may yield spurious Fourier components at the spatial frequencies of interest. Thus, we should not place undue quantitative trust in the calculated one-dimensional diffusion constants at low concentrations, though the computational artifacts are expected to become truly significant only in the range of concentrations for which spin diffusion is already nearly quenched. The presence of long-range dipole couplings, of course, serves to mitigate the situation. In any case, the diffusion constants as measured do serve as a practical gauge of the rate of dissipation of an initial inhomogeneity, and the general trends observed in this macroscopic index highlight the need for more detailed accountings of the microscopic geometry of the lattice.

IV. QUANTUM SPIN DYNAMICS AND SPIN COHERENT STATES

To this point, we have concerned ourselves entirely with classical spin diffusion. Our dynamical model has been one of classical gyromagnets precessing continuously under the influence of local magnetic fields. Nevertheless, the dynamics of interacting nuclear spins are, at root, quantum mechanical. What account can be made of the quantum origins of spin diffusion? The theoretical models of spin diffusion against which our classical simulations were tested are all quantum models. None of these models, however, affords a direct microscopic comparison with classical computational procedures. None is amenable to simulation at the level of individual spins.

We may make a preliminary case for the validity of the classical results by using the moment theory of Redfield and Yu (Sec. III and Ref. 5) to compare the predicted classical and quantum values of the spin diffusion constant for a fully populated lattice in high applied field. The quantum result is found to approach its classical counterpart rapidly with increasing spin quantum number, and even for spin-$\frac{1}{2}$, the quantum correction is only on the order of 0.5% to 4% of the total value (the proportion varies with the direction of the applied field).[10] This fact, combined with the observed agreement between quantum theories and classical simulations in certain test cases,[1,2,10] lends some credence to the classical model. Still, as was discussed in Sec. III, bulk parameters such as moments do not suffice to characterize all of the dynamics underlying spin diffusion.

In fact, the correspondence between classical and quantum spin diffusion may be demonstrated even at the microscopic level. This section is devoted to reconciling quantum theories with classical simulations using the interpolating properties of spin coherent states. Use of these states in formulating quantum dynamics affords a direct comparison with classical dynamical models. In the exposition to follow, a full quantum treatment of the spin diffusion problem will be shown to reduce precisely to the classical limit used in our simulations when the high-temperature limit is applied to lattices containing large numbers of coupled spins. Thus, we may have confidence not only in the bulk predictions of our classical simulations, but also in the underlying dynamical processes which these simulations bring to light.[22] It should be noted that although the specific case considered here involves spin diffusion mediated by dipole-dipole interactions, the equivalence of classical and quantum behaviors applies more generally for any set of interacting spins on a lattice which satisfies the broad conditions we will describe in this section.

A. The classical dynamical problem

Consider a regular array of N nuclear spins with magnetic moments $\{\boldsymbol{m}_j\}$ $(j = 1, 2, \ldots, N)$. Let us suppose that the spins in our model lattice are acted upon by a constant applied magnetic field $\boldsymbol{B}_0 = B_0\hat{z}$, and additionally are subject to dipole-dipole interactions. The energy

of such an arrangement is given in Eq. (2.3). Each spin, therefore, evolves under the influence of a local magnetic field which is the vector sum of the applied field and the dipole fields from all the other spins in the lattice. Under the action of spin-spin couplings, an initial disturbance in magnetization or interspin energy will diffuse across the lattice in accordance with Eqs. (2.1) and (2.2) until equilibrium is restored. A strategy for classical simulations of this dipole-mediated spin diffusion may be constructed as follows.

(1) Orient the spins $\{\boldsymbol{m}_j\}$ to produce an initial deviation from equilibrium. In Refs. 1, 2, and 10 a Boltzmann distribution was sampled for each spin orientation, with an effective local temperature which varied cosinusoidally across the lattice.

(2) Solve the coupled classical Bloch equations for all spins in the lattice. At each instant, the equation of motion for a spin $\boldsymbol{m}_j$ is

$$\begin{aligned} \dot{\boldsymbol{m}}_j(t) &= \boldsymbol{m}_j(t) \times \boldsymbol{B}_j(t), \\ \boldsymbol{B}_j(t) &= \sum_{k \neq j} \boldsymbol{B}_{jk}(t). \end{aligned} \tag{4.1}$$

The local field $\boldsymbol{B}_j$ is made up of contributions $\boldsymbol{B}_{jk}$ which depend upon the relative positions and the instantaneous relative orientations of spins $\boldsymbol{m}_j$ and $\boldsymbol{m}_k$.

(3) Calculate a diffusion constant from the rate of decay of the initial disturbance [cf. Eq. (2.2)].

The results of Secs. II and III were generated using this computational procedure. In fact, a wide range of dynamical situations may be addressed using a procedure of this general form, simply by altering the nature of the couplings, the particulars of the initial condition, or the measurable quantities to be computed.

B. The quantum dynamical problem

For a study of quantum spin dynamics, the classical dipoles $\{\boldsymbol{m}_j\}$ of Eq. (4.1) must be replaced by spin operators $\{\boldsymbol{I}_j\}$ with the usual commutation relations:

$$\begin{aligned} [I_{j_\alpha}, I_{k_\beta}] = i\delta_{jk}\epsilon_{\alpha\beta\zeta} I_{j_\zeta} \quad & j,k = 1,2,\ldots,N \\ & \alpha,\beta,\zeta = 1,2,3\ . \end{aligned} \tag{4.2}$$

Henceforward, we shall let $\hbar = 1$ and the gyromagnetic ratio $\gamma = 1$, unless the context demands otherwise. The spin quantum number, which we shall take to be the same for all spins in the lattice, will be referred to simply as I. The spatially inhomogeneous initial condition of the lattice may be represented by the density operator

$$\rho(0) = \frac{\exp\left(-\sum_j \beta_j I_{j_z}\right)}{\mathrm{Tr}\left\{\exp\left(-\sum_j \beta_j I_{j_z}\right)\right\}}, \tag{4.3}$$

where $\beta_j \equiv \hbar\omega_0/k_B T_j$, with $\hbar\omega_0$ a characteristic energy ($\omega_0 \sim -\gamma B_0$ in high field) and T_j a local spin "temperature" at lattice site j. In other words, we choose a local Boltzmann distribution for expected magnetization at each spin site, with site-to-site variations expressed as variations in the Boltzmann exponent β_j.

In order to characterize the transport of magnetization across the lattice, we seek average spin trajectories represented by the expectation values $\{\langle \boldsymbol{I}_j \rangle (t)\}$. The quantum equations of motion corresponding to the classical Bloch equations are

$$\frac{d\langle \boldsymbol{I}_j \rangle}{dt} = i\langle [\mathcal{H}, \boldsymbol{I}_j] \rangle = \langle \boldsymbol{I}_j \times \boldsymbol{B}_j \rangle\ . \tag{4.4}$$

Due to the noncommutation of the operators I_{j_x}, I_{j_y}, and I_{j_z}, $\langle \boldsymbol{I}_j \times \boldsymbol{B}_j \rangle \neq \langle \boldsymbol{I}_j \rangle \times \langle \boldsymbol{B}_j \rangle$ for a coupled spin system [since both $\boldsymbol{I}_j(t)$ and $\boldsymbol{B}_j(t)$ will in general depend in a complicated fashion upon all the components of $\boldsymbol{I}_j$, and noncommutation implies that the expectation value of products of operators will not equal the product of expectation values]. Consequently, classical differential equations do not suffice to describe the dynamics. On the other hand, it is not feasible to diagonalize quantum Hamiltonians for the large numbers of spins needed to model diffusion effects, and an alternative approach to quantum simulations is needed. The beginnings of such an approach can be constructed, and the connection between quantum and classical dynamics can be made explicit, by use of spin coherent states.

C. Spin coherent states

Unlike the standard basis of Zeeman states $|I,m\rangle$, spin coherent states[23–26] are an overcomplete set of states with the minimum uncertainty product allowed by the Heisenberg uncertainty relations. In this and other respects, they are analogous to the canonical coherent states for the harmonic oscillator. Radcliffe[23] identified this class of states in 1971, following the introduction of the canonical coherent states by Glauber in 1963.[27–29] Subsequent work has identified both of these state constructs as members of a family of "generalized coherent states" which may be built around arbitrary symmetry groups.[25,26,30]

The spin coherent states (SCS) are generated by rotations of a single base state, called the "fiducial state," chosen from the usual Hilbert space. They may be parametrized by a unit vector $\boldsymbol{n} = \sin\theta\cos\phi\hat{\boldsymbol{x}} + \sin\theta\sin\phi\hat{\boldsymbol{y}} + \cos\theta\hat{\boldsymbol{z}}$ as follows:

$$\begin{aligned} |\boldsymbol{n}\rangle &= D(\boldsymbol{n})\,|\Psi_0\rangle\,, \\ D(\boldsymbol{n}) &\equiv \exp[i\theta\,(-\sin\phi I_x + \cos\phi I_y)], \end{aligned} \tag{4.5}$$

where $|\Psi_0\rangle$ is a state $|I,m\rangle$ in the Zeeman basis. As a consequence of this definition, it is clear that the SCS wave packets undergo no spreading with rotation. An arbitrary rotation $T(R)$ maps one coherent state $|\boldsymbol{n}\rangle$ smoothly onto a rotated coherent state $|R\boldsymbol{n}\rangle$. This mapping involves a phase factor discussed further elsewhere,[31] but no mixing of the SCS occurs.

If in particular we choose the stretched state $|I,I\rangle$ as our fiducial state $|\Psi_0\rangle$, the Heisenberg uncertainty relation for the components of I is saturated.[32] In order better to visualize these minimal-uncertainty states, we may decompose them in the usual Zeeman basis:[23]

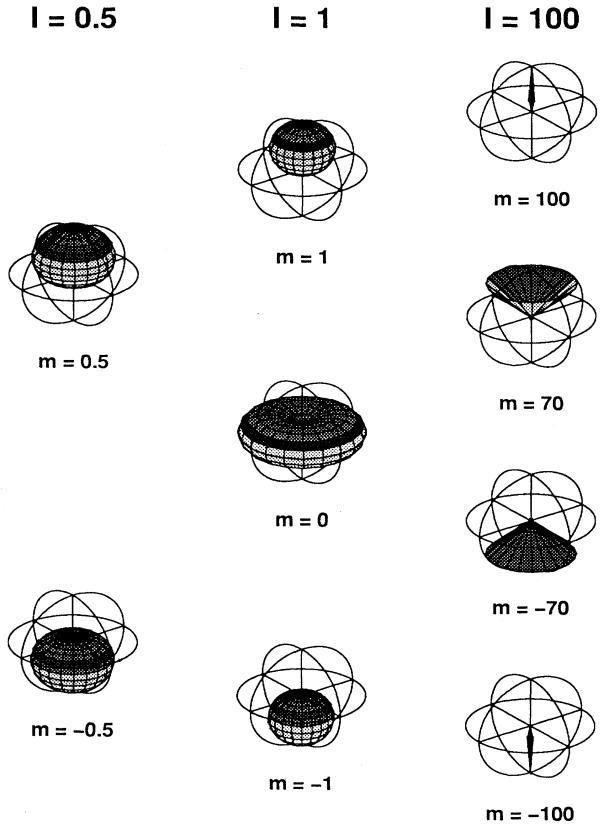

FIG. 8. Angular plot of the overlap of spin coherent states with the usual Zeeman states. The function $|\Psi_m(\theta,\phi)|^2 \equiv |\langle I,m|\boldsymbol{n}\rangle|^2$ (normalized to the unit sphere) is plotted for various I and m.

$$|\boldsymbol{n}\rangle = \sum_m |I,m\rangle\,\langle I,m|\boldsymbol{n}\rangle$$

$$\langle I,m|\boldsymbol{n}\rangle = \begin{pmatrix} 2I \\ I-m \end{pmatrix}^{\frac{1}{2}} \left(\cos\frac{\theta}{2}\right)^{I+m} \left(\sin\frac{\theta}{2}\right)^{I-m} \times \exp[i\,(I-m)\,\phi]. \tag{4.6}$$

In Fig. 8, the square magnitude of the overlap $|\Psi_m(\theta,\phi)|^2 \equiv |\langle I,m|\boldsymbol{n}\rangle|^2$ is plotted as a function of θ and ϕ for a variety of I and m values. The function $|\Psi_m(\theta,\phi)|^2$ is a probability density function describing a distribution of vector orientations peaked at $\cos\theta = \frac{m}{I}$. One may observe that in the quantum limit ($I = \frac{1}{2}$), the distributions are broad, and a wide range of SCS vector orientations are contained in $|I,m\rangle$, whereas $|\Psi_m|^2$ collapses to well-defined cones in the classical limit of large I. It can be argued that the cones define an expected orientational distribution for pure states $|I,m\rangle$, and the collapse of the overlap probability to this base distribution implies that in the vicinity of the classical limit, the SCS are essentially angular delta functions, better known as classical vectors.

In short, the spin coherent states $\{|\boldsymbol{n}\rangle\}$ represent spin wave functions of minimal width centered about the classical vectors $\{I\boldsymbol{n}\}$, and they maintain their coherent character under unitary rotations. In these respects, they are an appealing analogue for classical spins. They may indeed be said to be the most "classical" of allowed quantum spin states—the closest one can get while still respecting quantum constraints. As such, they have been used to explore the classical limit of quantum spin systems[33,34] and to formulate path integrals for interacting spins.[35–39]

Some useful features of spin coherent states are summarized below (following Perelomov in Ref. 26 and Radcliffe in Ref. 23):

1. Overcompleteness

$$\langle \boldsymbol{n}'|\boldsymbol{n}\rangle = \left(\cos\frac{\theta}{2}\cos\frac{\theta'}{2} + \sin\frac{\theta}{2}\sin\frac{\theta'}{2}e^{i(\phi-\phi')}\right)^{2I} = \exp[iIA\,(\boldsymbol{n}',\boldsymbol{n},\boldsymbol{n}_0)]\left(\frac{1+\boldsymbol{n}\cdot\boldsymbol{n}'}{2}\right)^{I}. \tag{4.7}$$

$A\,(\boldsymbol{n}',\boldsymbol{n},\boldsymbol{n}_0)$ is the area of the geodesical triangle formed by the vertices $\boldsymbol{n}'$, $\boldsymbol{n}$, and $\boldsymbol{n}_0 = \hat{\boldsymbol{z}}$.

2. Resolution of unity

$$\mathbb{1} = \int d\mu|\boldsymbol{n}\rangle\langle\boldsymbol{n}|,$$

$$d\mu = \frac{2I+1}{4\pi}\sin\theta d\theta d\phi = \frac{2I+1}{4\pi}d\Omega. \tag{4.8}$$

3. Diagonal representation of operators

Any bounded operator A in the Hilbert space admits a diagonal representation in terms of spin coherent states

$$A = \int d\mu\mathcal{A}(\boldsymbol{n})|\boldsymbol{n}\rangle\langle\boldsymbol{n}|. \tag{4.9}$$

When A is equal to the spin operator I, the diagonal symbol $\mathcal{A}(\boldsymbol{n}) \equiv \mathcal{I}(\boldsymbol{n})$ takes a particularly simple form:

$$\mathcal{I}(\boldsymbol{n}) = (I+1)\boldsymbol{n}. \tag{4.10}$$

4. Operator matrix elements in the spin coherent state representation

$$\langle\boldsymbol{n}|\,\boldsymbol{I}\,|\boldsymbol{n}\rangle = I\boldsymbol{n},$$

$$\langle\boldsymbol{n}'|\,\boldsymbol{I}\,|\boldsymbol{n}\rangle = \langle\boldsymbol{n}'|\boldsymbol{n}\rangle\; I\,\frac{\boldsymbol{n}+\boldsymbol{n}'+i\,(\boldsymbol{n}\times\boldsymbol{n}')}{1+\boldsymbol{n}\cdot\boldsymbol{n}'} \equiv \langle\boldsymbol{n}'|\boldsymbol{n}\rangle\; I\boldsymbol{\eta}\,(\boldsymbol{n},\boldsymbol{n}'),$$

$$\langle\boldsymbol{n}|\,e^{-\beta I_z}\,|\boldsymbol{n}\rangle = \left(\cosh\frac{\beta}{2} - \sinh\frac{\beta}{2}\,\cos\theta\right)^{2I},$$

$$\langle\boldsymbol{n}'|\,e^{-\beta I_z}\,|\boldsymbol{n}\rangle = \langle\boldsymbol{n}'|\boldsymbol{n}\rangle\left(\cosh\frac{\beta}{2} - \sinh\frac{\beta}{2}\,\eta_z\right)^{2I}. \tag{4.11}$$

5. Traces

$$\mathrm{Tr}\,\{A\} = \int d\mu\,\langle\boldsymbol{n}|\,A\,|\boldsymbol{n}\rangle = \int d\mu\mathcal{A}(\boldsymbol{n}). \tag{4.12}$$

6. Product rule for traces

$$\begin{aligned}\mathrm{Tr}\{AB\} &= \int d\mu \langle \boldsymbol{n}| AB |\boldsymbol{n}\rangle \\ &= \int d\mu' \mathcal{A}(\boldsymbol{n}') \langle \boldsymbol{n}'| B |\boldsymbol{n}'\rangle \\ &= \int d\mu' \mathcal{B}(\boldsymbol{n}') \langle \boldsymbol{n}'| A |\boldsymbol{n}'\rangle . \end{aligned} \tag{4.13}$$

D. Spin coherent states and quasiclassical quantum dynamics

In order to compare classical and quantum spin diffusion, we first express the quantum equations of motion (4.4) in terms of spin coherent states. Choosing the Heisenberg picture, in which the states and the density matrix are constant while the operators evolve, we write

$$\mathrm{Tr}\left\{\rho(0)\dot{\boldsymbol{I}}_j(t)\right\} = \mathrm{Tr}\{\rho(0)\boldsymbol{I}_j(t) \times \boldsymbol{B}_j(t)\}. \tag{4.14}$$

Since the operators representing spins at different lattice sites commute at time zero, we may decompose a state of the lattice into a direct product of states for individual spin sites. For spin coherent states in particular,

$$|\{\boldsymbol{n}\}\rangle \equiv \bigotimes_j |\boldsymbol{n}_j\rangle . \tag{4.15}$$

Now we use the trace formulas of Sec. IV C, with the notation $d\{\mu\} \equiv \prod_k d\mu_k$. The left-hand side of Eq. (4.14) is

$$\mathrm{Tr}\left\{\rho(0)\dot{\boldsymbol{I}}_j(t)\right\} = \int d\{\mu\}\ \langle\{\boldsymbol{n}\}|\, \rho(0)\, |\{\boldsymbol{n}\}\rangle\ \dot{\boldsymbol{\mathcal{I}}}_j(\{\boldsymbol{n}\},t). \tag{4.16}$$

The right-hand side may be expanded as follows:

$$\begin{aligned}\mathrm{Tr}\{\rho(0)\boldsymbol{I}_j \times \boldsymbol{B}_j\} &= \int d\{\mu\}\ \langle\{\boldsymbol{n}\}|\, \rho(0)\, \boldsymbol{I}_j(t) \times \boldsymbol{B}_j(t)\ |\{\boldsymbol{n}\}\rangle \\ &= \int d\{\mu\}\, d\{\mu'\}\ \langle\{\boldsymbol{n}\}|\, \rho(0)\ |\{\boldsymbol{n}'\}\rangle\ \boldsymbol{\mathcal{I}}_j(\{\boldsymbol{n}'\},t) \times \langle\{\boldsymbol{n}'\}|\ \boldsymbol{B}_j(t)\ |\{\boldsymbol{n}\}\rangle \\ &= \int d\{\mu\}\, d\{\mu'\}\, d\{\mu''\}\ \langle\{\boldsymbol{n}\}|\, \rho(0)\ |\{\boldsymbol{n}'\}\rangle\ \langle\{\boldsymbol{n}'\}\,|\,\{\boldsymbol{n}''\}\rangle\ \langle\{\boldsymbol{n}''\}\,|\,\{\boldsymbol{n}\}\rangle \boldsymbol{\mathcal{I}}_j(\{\boldsymbol{n}'\},t) \times \boldsymbol{\mathcal{B}}_j(\{\boldsymbol{n}''\},t) \\ &= \int d\{\mu'\}\, d\{\mu''\}\ \langle\{\boldsymbol{n}''\}|\, \rho(0)\ |\{\boldsymbol{n}'\}\rangle\ \langle\{\boldsymbol{n}'\}\,|\,\{\boldsymbol{n}''\}\rangle\ \boldsymbol{\mathcal{I}}_j(\{\boldsymbol{n}'\},t) \times \boldsymbol{\mathcal{B}}_j(\{\boldsymbol{n}''\},t). \end{aligned} \tag{4.17}$$

The final contraction in (4.17) is achieved by moving the factor $\langle\{\boldsymbol{n}''\}\,|\,\{\boldsymbol{n}\}\rangle$ to the front of the integrand and removing a resolution of unity: $\int d\{\mu\}\,|\{\boldsymbol{n}\}\rangle\langle\{\boldsymbol{n}\}|$. Combining left-hand and right-hand expressions, and relabeling integration indices, we arrive at the equation

$$\int d\{\mu\}\,\langle\{\boldsymbol{n}\}|\,\rho(0)\,|\{\boldsymbol{n}\}\rangle \dot{\boldsymbol{\mathcal{I}}}_j(\{\boldsymbol{n}\},t) = \int d\{\mu\}\, d\{\mu'\}\ \langle\{\boldsymbol{n}\}\,|\,\{\boldsymbol{n}'\}\rangle\ \langle\{\boldsymbol{n}'\}|\ \rho(0)\ |\{\boldsymbol{n}\}\rangle\ \boldsymbol{\mathcal{I}}_j(\{\boldsymbol{n}\},t) \times \boldsymbol{\mathcal{B}}_j(\{\boldsymbol{n}'\},t). \tag{4.18}$$

Solution of this integrodifferential expression for the spin symbols $\boldsymbol{\mathcal{I}}_j(\{\boldsymbol{n}\},t)$ constitutes a complete solution of the problem, since with the symbols in hand we may immediately calculate the desired expectation values,

$$\langle \boldsymbol{I}_j\rangle(t) = \mathrm{Tr}\{\rho(0)\boldsymbol{I}_j(t)\} = \int d\{\mu\}\,\langle\{\boldsymbol{n}\}|\,\rho(0)\,|\{\boldsymbol{n}\}\rangle\ \boldsymbol{\mathcal{I}}_j(\{\boldsymbol{n}\},t). \tag{4.19}$$

Equation (4.18) as written is difficult to solve. If our initial lattice configuration is such that the density operator $\rho(0)$ admits the following approximation,

$$\langle\{\boldsymbol{n}\}\,|\,\{\boldsymbol{n}'\}\rangle\ \langle\{\boldsymbol{n}'\}|\ \rho(0)\ |\{\boldsymbol{n}\}\rangle \approx \langle\{\boldsymbol{n}\}\,|\,\{\boldsymbol{n}'\}\rangle \langle\{\boldsymbol{n}'\}\,|\,\{\boldsymbol{n}\}\rangle\ \langle\{\boldsymbol{n}\}|\ \rho(0)\ |\{\boldsymbol{n}\}\rangle, \tag{4.20}$$

a substantial simplification may be achieved. Inserting expression (4.20) into (4.18) above, and identifying a diagonal representation of the local field operator $\boldsymbol{B}_j(t) = \int d\{\mu'\}\,\boldsymbol{\mathcal{B}}_j(\{\boldsymbol{n}'\},t)\ |\{\boldsymbol{n}'\}\rangle\langle\{\boldsymbol{n}'\}|$, we obtain

$$\int d\{\mu\}\,\langle\{\boldsymbol{n}\}|\,\rho(0)\,|\{\boldsymbol{n}\}\rangle \dot{\boldsymbol{\mathcal{I}}}_j(\{\boldsymbol{n}\},t) \approx \int d\{\mu\}\ \langle\{\boldsymbol{n}\}|\ \rho(0)\ |\{\boldsymbol{n}\}\rangle\ \boldsymbol{\mathcal{I}}_j(\{\boldsymbol{n}\},t) \times \langle\{\boldsymbol{n}\}|\,\boldsymbol{B}_j(t)\,|\{\boldsymbol{n}\}\rangle . \tag{4.21}$$

The form of $\rho(0)$ is arbitrary, at least within the constraints of the approximation (4.20), so that we may equate the integrands

$$\dot{\boldsymbol{\mathcal{I}}}_j(\{\boldsymbol{n}\},t) \approx \boldsymbol{\mathcal{I}}_j(\{\boldsymbol{n}\},t) \times \langle\{\boldsymbol{n}\}|\,\boldsymbol{B}_j(t)\,|\{\boldsymbol{n}\}\rangle . \tag{4.22}$$

At time $t = 0$, the Heisenberg operators $\boldsymbol{I}_j(t)$ coincide with the usual spin operators $\boldsymbol{I}_j$, and the symbols are simply $\boldsymbol{\mathcal{I}}_j(\{\boldsymbol{n}\},0) = (I+1)\boldsymbol{n}_j$. The diagonal matrix elements of the local field operator $\langle\{\boldsymbol{n}\}|\,\boldsymbol{B}_j(0)\,|\{\boldsymbol{n}\}\rangle$ reduce to the classical functions $\boldsymbol{B}_j(\{I\boldsymbol{n}\},0)$, with each spin component I_{k_α} in the operator expression replaced by the corresponding component of a classical vector In_{k_α}. The result is

$$\dot{\boldsymbol{n}}_j(0) \approx \boldsymbol{n}_j(0) \times \boldsymbol{B}_j(\{I\boldsymbol{n}\},0). \tag{4.23}$$

This equation is just the familiar classical Bloch equation evaluated at time zero. Consequently, the time-dependent functions $I\boldsymbol{n}_j(t)$ will evolve precisely as classical spin vectors $\boldsymbol{m}_j(t)$ for all time, subject to the classical equations of motion

$$\dot{\boldsymbol{m}}_j(t) \approx \boldsymbol{m}_j(t) \times \boldsymbol{B}_j(t)\ . \tag{4.24}$$

With the determination of $\boldsymbol{\mathcal{I}}_j(\{\boldsymbol{n}\},t)$ [which simply equals $(I+1)\ \boldsymbol{n}_j(\{\boldsymbol{n}\},t)$] having proceeded along classical lines, only integration against the weight function $\langle\{\boldsymbol{n}\}|\,\rho(0)\,|\{\boldsymbol{n}\}\rangle$ remains [cf. Eq. (4.19)]. Referring to Eq. (4.3) and substituting the diagonal matrix elements of Eq. (4.11) gives

$$\begin{aligned}\langle\{\boldsymbol{n}\}|\,\rho(0)\,|\{\boldsymbol{n}\}\rangle &= \frac{\langle\{\boldsymbol{n}\}|\exp\left(-\sum_j \beta_j I_{j_z}\right)|\{\boldsymbol{n}\}\rangle}{\mathrm{Tr}\left\{\exp\left(-\sum_j \beta_j I_{j_z}\right)\right\}} \\ &= \prod_j \frac{\left(\cosh\frac{\beta_j}{2} - \sinh\frac{\beta_j}{2}\ \cos\theta_j\right)^{2I}}{\frac{2I+1}{2}\int d\cos\theta_j \left(\cosh\frac{\beta_j}{2} - \sinh\frac{\beta_j}{2}\ \cos\theta_j\right)^{2I}}.\end{aligned} \tag{4.25}$$

In the high-temperature limit ($\beta_j \ll 1$), this function reduces to a Boltzmann distribution

$$\langle\{\boldsymbol{n}\}|\,\rho(0)\,|\{\boldsymbol{n}\}\rangle \overset{\beta_j\ll 1}{\longrightarrow} \prod_j \frac{\exp\left(-\beta_j I\cos\theta_j\right)}{\int d(I\cos\theta_j)\exp\left(-\beta_j I\cos\theta_j\right)}, \tag{4.26}$$

where $I\cos\theta_j$ plays the role of z component of a classical magnetization vector. We may then view the expectation value expression as an ensemble integral over a classical lattice. Since we are ultimately interested in a bulk parameter rather than the true ensemble average of any individual spin magnetization, we may select one or several representative lattice configurations and evaluate the spin diffusion constant. The correspondence with the classical calculations is now complete.

Under what physical conditions is the approximation (4.20) valid? Let us first consider the classical limit, in which we naturally expect our quantum model to yield classical equations of motion. The expression (4.11) for the off-diagonal elements of an exponential spin operator gives

$$\langle\{\boldsymbol{n}\}\,|\,\{\boldsymbol{n}'\}\rangle\ \langle\{\boldsymbol{n}'\}|\ \rho(0)\ |\{\boldsymbol{n}\}\rangle = \langle\{\boldsymbol{n}\}\,|\,\{\boldsymbol{n}'\}\rangle\,\langle\{\boldsymbol{n}'\}\,|\,\{\boldsymbol{n}\}\rangle\,\frac{\prod_j\left(\cosh\frac{\beta_j}{2} - \sinh\frac{\beta_j}{2}\ \eta_{j_z}\right)^{2I}}{\mathrm{Tr}\left\{\exp\left(-\sum_j \beta_j I_{j_z}\right)\right\}}, \tag{4.27}$$

with the complex vector $\boldsymbol{\eta}_j$ defined as in Eq. (4.11):

$$\boldsymbol{\eta}_j \equiv \frac{\boldsymbol{n}_j + \boldsymbol{n}'_j + i\left(\boldsymbol{n}_j \times \boldsymbol{n}'_j\right)}{1 + \boldsymbol{n}_j \cdot \boldsymbol{n}'_j}. \tag{4.28}$$

For large spin quantum number I, the prefactor $|\langle\{\boldsymbol{n}\}\,|\,\{\boldsymbol{n}'\}\rangle|^2 = \prod_j\left[\left(1+\boldsymbol{n}_j\cdot\boldsymbol{n}'_j\right)/2\right]^{2I}$ vanishes for all $\boldsymbol{n}'_j$ which are not very near $\boldsymbol{n}_j$, while the resolution of unity (4.8) guarantees a unit integral. Thus, the prefactor approaches a product of delta functions $\prod_j \delta(\boldsymbol{n}'_j - \boldsymbol{n}_j)$, and η_{j_z} may be replaced by $\cos\theta_j$, justifying the classical approximation. These arguments show how the disappearance of complex interference terms accompanies the classical limit. The expectation value expressions for quantum spin operators in the SCS representation contract smoothly to classical values as the spin quantum number is increased.[40]

For small I, closer to the "quantum limit" of $I = \frac{1}{2}$ realized in physical systems such as CaF_2 crystals, there is considerable latitude in the values of $\{\boldsymbol{n}'\}$, and the complex terms in η_{j_z} may not be ignored. Nevertheless, under certain conditions, cancellations allow us to recover the classical results. At the high temperatures which are standard in many NMR experiments ($T \sim 300°$, $\beta \sim 10^{-5}$ for fields of several T), the exponential density operator may be expanded to first order in β, yielding the following expression for the left-hand side of (4.20):

$$\begin{aligned}\langle\{\boldsymbol{n}\}\,|\,\{\boldsymbol{n}'\}\rangle\ \langle\{\boldsymbol{n}'\}|\,\rho(0)\,|\{\boldsymbol{n}\}\rangle &\overset{\beta_j\ll 1}{\longrightarrow} \langle\{\boldsymbol{n}\}\,|\,\{\boldsymbol{n}'\}\rangle\ \langle\{\boldsymbol{n}'\}|\,\frac{\mathbb{1} - \sum_j \beta_j I_{j_z}}{\mathrm{Tr}\left\{\exp\left(-\sum_j \beta_j I_{j_z}\right)\right\}}\,|\{\boldsymbol{n}\}\rangle \\ &= \langle\{\boldsymbol{n}\}\,|\,\{\boldsymbol{n}'\}\rangle\,\langle\{\boldsymbol{n}'\}\,|\,\{\boldsymbol{n}\}\rangle\,\frac{1 - \sum_j \beta_j \eta_{j_z}}{\mathrm{Tr}\left\{\exp\left(-\sum_j \beta_j I_{j_z}\right)\right\}}.\end{aligned} \tag{4.29}$$

If the spatial variation in β_j is slow enough that many spins lie together in regions of nearly uniform spin temperature, then the imaginary terms in η_{j_z} for different spins in each subregion tend to interfere with one another, and the real terms tend to accumulate to an average value somewhat less than $\sum_j \cos\theta_j$. The result is that the sum is "buffered" against variations in $\{\boldsymbol{n}'\}$, and the predominant $\{\boldsymbol{n}'\}$ dependence lies in the prefactor $|\langle\{\boldsymbol{n}\}\,|\,\{\boldsymbol{n}'\}\rangle|^2$. At the expense of a partial reduction in the effective magnitude of β_j for each subregion of the lattice, we may replace (4.29) with

$$\begin{aligned}\langle\{\boldsymbol{n}\}\,|\,\{\boldsymbol{n}'\}\rangle\ \langle\{\boldsymbol{n}'\}|\,\rho(0)\,|\{\boldsymbol{n}\}\rangle &\approx \langle\{\boldsymbol{n}\}\,|\,\{\boldsymbol{n}'\}\rangle\,\langle\{\boldsymbol{n}'\}\,|\,\{\boldsymbol{n}\}\rangle\,\frac{1-\sum_j \bar{\beta}_j\cos\theta_j}{\mathrm{Tr}\left\{\exp\left(-\sum_j \beta_j I_{j_z}\right)\right\}} \\ &\approx \langle\{\boldsymbol{n}\}\,|\,\{\boldsymbol{n}'\}\rangle\,\langle\{\boldsymbol{n}'\}\,|\,\{\boldsymbol{n}\}\rangle\ \langle\{\boldsymbol{n}\}|\ \rho(0)\ |\{\boldsymbol{n}\}\rangle\,, \end{aligned} \tag{4.30}$$

and (4.20) is satisfied. In the long-wavelength, high-temperature limit, we expect the quantum results to be well approximated by classical calculations, even for spins as low as $I = 1/2$.

A more complete assessment of the size and character of quantum corrections to the classical dynamical model may be possible using the SCS formalism. For example, one might imagine expanding expressions such as Eq. (4.18) in powers of β. The resulting integrals over $\{\boldsymbol{n}'\}$ for corrections of first and higher orders suggest a model of interacting "virtual lattices," in which spins respond not only to other spins in their home lattice $\{\boldsymbol{n}\}$ but also to spins in a suitably chosen set of accessory lattices $\{\boldsymbol{n}'\}$. Such a construction would be reminiscent of the Trotter-Suzuki style of path integration for spin systems, which maps the quantum problem to an equivalent classical problem of higher dimensionality.[41–44] Takano[37,38] has designed a strategy for path integration using the SCS, and this strategy might well be modified to form a dynamical path integral (though for reasons of convergence this strategy is likely to be successful only for small numbers of interacting spins). The work of Takahashi and Shibata[45,46] (who derive differential operator equations for spin distribution functions using product rules for diagonal symbols) might also be extended to large systems of dipole-coupled spins, though substantial approximations might be required to render the mathematics tractable.

V. CONCLUSIONS

Given the isotropic nature of the dipole-dipole Hamiltonian in zero applied field, the question of how an anisotropic disturbance in a spin lattice will dissipate might at first invite some speculation: will it merely decay in amplitude with its anisotropy preserved, or will it be dispersed in orientation as well? Our results suggest that the answer depends upon the nature of the disturbance. If it is a conserved quantity that we perturb in setting up our initial condition, then that quantity diffuses along local gradients in a well-behaved fashion, with its orientational character maintained over time. The breakdown of diffusive behavior for longitudinal magnetization in zero field, and the corresponding orientational mixing which dominates the dynamics in this case, is explained by the simple observation that the zero-field dipole Hamiltonian does not conserve spin angular momentum.

In lattices at high applied field, diffusion is hindered by dilution to a degree that depends both upon the concentration of spins and upon their spatial distribution. Section III demonstrates that the concentration dependence observed in simulated lattices with various dimensionalities may be characterized at least in a qualitative fashion using combinations of moment theory, simple scaling arguments, and observations of percolation in simplified systems.

Finally, in Sec. IV, we have offered theoretical evidence as to why classical results should indeed be faithful guides for our more quantum mechanical expectations. Under physical conditions of some practical interest—namely, in macroscopic lattices at or above room temperature—spin coherent state expectation value expressions may be manipulated to recover classical equations of motion. The disappearance of quantum interference terms under these conditions justifies the use of classical simulations in studies of spin diffusion or similar magnetic phenomena in lattices. In the context of the SCS formalism, the nature and effect of quantum interferences becomes particularly palpable. Thus, the SCS may be used to forge a practical as well as a conceptual link between classical and quantum spin dynamics.

ACKNOWLEDGMENTS

We thank Dr. I. Nolden for data that served as helpful guides for our simulations of diluted lattices. We have also profited from communications with Dr. Nolden and from discussions with Dr. R. J. Silbey. This work was supported in part by the National Science Foundation.

[1] C. Tang and J. S. Waugh, Phys. Rev. B **45**, 748 (1992).
[2] C. Tang, Ph.D. dissertation, Massachusetts Institute of Technology, Department of Chemistry, 1990.
[3] N. Bloembergen, Physica (Utrecht) **15**, 386 (1949).
[4] A. G. Redfield, Phys. Rev. **116**, 315 (1959).
[5] A. G. Redfield and W. N. Yu, Phys. Rev. **169**, 443 (1968); **177**, 1018 (1969).
[6] I. J. Lowe and S. Gade, Phys. Rev. **156**, 817 (1967); **166**,

934 (1968).
[7] P. Borckmans and D. Walgraef, Phys. Rev. **167**, 282 (1968).
[8] T. Morita, Phys. Rev. B **6**, 3385 (1972).
[9] References to experimental studies of spin diffusion may be found in Ref. 1.
[10] D. K. Sodickson, Ph.D. dissertation, Massachusetts Institute of Technology, Harvard-MIT Division of Health Sciences and Technology, 1994.
[11] For reasons of convenience and generality, reduced units have been used in all the calculations. The nearest-neighbor distance r_0 and the magnetic moment m of a single spin are scaled to unity, as is the gyromagnetic ratio γ. Time is measured in units of $r_0^3/|\gamma m|$ (the inverse of the nearest-neighbor dipole coupling strength). Diffusion constants have units of $|\gamma m|/r_0$. In a CaF_2 crystal, these units amount to 35.1×10^{-6} s and 2.12×10^{-15} m^2 s^{-1}, respectively.
[12] The traditional high-field truncation is performed by transforming to a rotating frame at the Larmor frequency $\omega_0 = -\gamma B_0$ and averaging all terms with a transverse phase dependence. This procedure eliminates the trivial $\boldsymbol{m}_j \cdot \boldsymbol{B}_0$ term and preserves only the T_0^2 component in the tensor expansion of the remaining dipolar Hamiltonian, resulting in Eq. (2.4).
[13] D. L. Huber, J. Phys. Chem. Solids **32**, 2145 (1971).
[14] E. Frey, F. Schwabl, and S. Thoma, Phys. Rev. B **40**, 7199 (1989).
[15] S. W. Lovesey, J. Phys. Condens. Matter. **5**, L251 (1993).
[16] I. Nolden and R. J. Silbey (private communication).
[17] I. Nolden and R. J. Silbey (unpublished).
[18] J. H. Van Vleck, Phys. Rev. **74**, 1168 (1948).
[19] C. Kittel and E. Abrahams, Phys. Rev. **90**, 238 (1953).
[20] D. Stauffer, *Introduction to Percolation Theory* (Taylor and Francis, London, 1985).
[21] By contrast, detailed studies have been made of the thermodynamic and kinetic properties of dilute magnetic systems subject to *local* interactions such as exchange couplings. Cf. R. B. Stinchcombe, in *Phase Transitions and Critical Phenomena*, edited by C. Domb and J. L. Lebowitz (Academic Press, London, 1983), Vol. 7, p. 151.
[22] That the computational lattices used in our classical simulations are consistent with the high-temperature, many-particle, long-wavelength limit has been demonstrated in Refs. 1, 2, and 10.
[23] J. M. Radcliffe, J. Phys. A **4**, 313 (1971).
[24] F. T. Arecchi, E. Courtens, R. Gilmore, and H. Thomas, Phys. Rev. A **6**, 2211 (1972).
[25] J. R. Klauder and B. S. Skagerstam, *Coherent States* (World Scientific, Singapore, 1985), pp. 25–38.
[26] A. Perelomov, *Generalized Coherent States and Their Applications* (Springer-Verlag, Berlin, 1986), Chap. 4.
[27] R. J. Glauber, Phys. Rev. Lett. **10**, 84 (1963).
[28] R. J. Glauber, Phys. Rev. **130**, 2529 (1963).
[29] R. J. Glauber, Phys. Rev. **131**, 2766 (1963).
[30] W. M. Zhang, D. H. Feng, and R. Gilmore, Rev. Mod. Phys. **62**, 867 (1990).
[31] D. K. Sodickson and J. S. Waugh (unpublished).
[32] $|\Psi_0\rangle = |I, -I\rangle$ is also an optimal choice of fiducial vector, and is distinguished from our choice by a change of sign in various matrix elements. Radcliffe (Ref. 23) uses $|I, I\rangle$ as his starting vector, whereas Perelomov (Ref. 26) chooses $|I, -I\rangle$.
[33] E. H. Lieb, Commun. Math. Phys. **31**, 327 (1973).
[34] D. V. Kapor, M. J. Skrinjar, and S. D. Stojanovic, Phys. Rev. B **44**, 2227 (1991).
[35] J. R. Klauder, Phys. Rev. D **19**, 2349 (1979).
[36] H. Kuratsuji and T. Suzuki, J. Math. Phys. **21**, 472 (1980).
[37] H. Takano, Prog. Theor. Phys. **73**, 332 (1985).
[38] H. Takano, in *Quantum Monte Carlo Methods in Equilibrium and Nonequilibrium Systems*, edited by M. Suzuki (Springer-Verlag, Berlin, 1987), p. 144.
[39] M. Bergeron, Fortschr. Phys. **40**, 119 (1992).
[40] Strictly speaking, the classical limit involves letting $\hbar \to 0$ as $I \to \infty$, with $\sqrt{I(I+1)}\hbar = \text{const}$. Since we have already invoked the high-temperature limit in treating our initial condition ($\beta\hbar \to 0$), this condition is effectively satisfied. For low temperatures, differences between the quantum and the classical initial conditions might become manifest.
[41] M. Suzuki, Commun. Math. Phys. **51**, 183 (1976).
[42] M. Suzuki, Prog. Theor. Phys. **56**, 1454 (1976).
[43] M. Suzuki, S. Miyashita, and A. Kuroda, Prog. Theor. Phys. **58**, 1377 (1977).
[44] M. Suzuki, in *Quantum Monte Carlo Methods in Equilibrium and Nonequilibrium Systems* (Ref. 38), p. 2.
[45] Y. Takahashi and F. Shibata, J. Stat. Phys. **14**, 49 (1976).
[46] Y. Takahashi and F. Shibata, J. Phys. Soc. Jpn. **38**, 656 (1975).